Photoswitchable auxin-inducible degron system for conditional protein degradation with spatiotemporal resolution

Saugata Sahu[a], Koya Yoshizawa[b], Takahiro Yamamoto[b], Ryota Uehara[b,c], Nobuyuki Tamaoki[a,b]*

[a]Research Institute for Electronic Science, Hokkaido University, Sapporo 001-0020, Japan. [b]Graduate School of Life Science, Hokkaido University, Sapporo 060-0810, Japan. [c]Faculty of Advanced Life Science, Hokkaido University, Sapporo 060-0810, Japan

*Email: tamaoki@es.hokudai.ac.jp

ABSTRACT: The auxin-inducible degron (AID) system degrades target proteins rapidly in a controllable manner. Although this is a highly versatile technique for studying protein functionality, protein degradation with spatiotemporal resolution is not currently possible. Herein, we describe a photoswitchable AID using a light active auxin derivative for reversible and site-specific protein degradation with temporal resolution.

Conditional protein depletion is a powerful technique to study protein functionalities.[1,2] The auxin-inducible degron (AID) system is extensively used to harness conditional protein degradation.[3–9] In non-plant cells expressing *Oryza sativa* TIR1 (OsTIR1)-modified E3-ligase exogenously, the protein of interest (POI) fused with mini-Auxin-inducible degron (mAID) tag is effectively degraded in the presence of the auxin ligand.[10] The ligand acts as a molecular glue between the degron-tagged POI and E3-ligase to degrade the protein by inducing the proximal ubiquitination of the POI. Protein functionality in complex biological systems has been studied using the AID system owing to its i) highly specific, rapid, and complete protein degradation abilities in the cytoplasm and nucleus of human cells and ii) reversible nature that can be immediately restored by removing the ligand.[5,10] Although AID is an excellent method for studying protein functionality, spatial control of protein degradation, such as targeted degradation in specific cells in a cell population, is impossible. Moreover, washing the auxin ligand to achieve reversibility is not a rational choice when continuous data acquisition is necessary with a stable medium to monitor a real-time dynamic biological process. Our group and others have achieved spatiotemporal control over various biological systems by integrating molecular photoswitches into the structure of biologically active small molecules[11-13] including proteolysis targeting chimeras (PROTACs)[14–17] which are deeply relevant to the present work.

Herein, we describe a photoswitchable AID (PAID) system, using a photoswitchable auxin to facilitate precise spatiotemporal control of conditional protein degradation. The auxin derivative was photoswitched reversibly between an agonist and antagonist depending on the wavelength of irradiation light, which degraded proteins with a remarkable 325-fold change in the half-maximal effective concentration (EC_{50}) values. Proteins were degraded in a site-specific manner with a spatial resolution of several hundred micrometers. Furthermore, protein degradation and subsequent re-expression were reversibly controlled simply by altering the irradiated light conditions without requiring to change the medium.

5-Phenyl-indole-3-acetic acid and $OsTIR1^{F74G}$-E3 ligase induced a rapid and target-specific AID-based protein degradation with nanomolar ligand concentrations.[17] A bump-and-hole strategy achieved by creating a suitable auxin with a bump and the genetically engineered TIR1 with a hole orthogonally triggers auxin signaling in vivo both at the transcriptomic level and in specific developmental contexts without interfering with endogenous auxin.[18] We hypothesized that conditional protein degradation with spatiotemporal resolution could be achieved with structurally dissimilar photoisomers via the orthogonal binding approach (Figure 1a). We separately introduced a phenylazo moiety at the 5- and 6-positions of indole-3-acetic acid (IAA) to obtain photoswitchable 5-phenylazo-IAA (**1**) and 6-phenylazo-IAA (**2**), respectively (Figures 1b and 1c), which were characterized via proton (^{1}H) and carbon (^{13}C)-nuclear magnetic resonance (NMR) and electrospray ionization (ESI) mass spectroscopy (Figures S22–S38). The photophysical properties and photoisomerization of **1** and **2** were analyzed in acetonitrile at 25 °C (Figures 1d–f, S1, S2 and Table S1). *E*-**1** and *E*-**2** show a strong π–π* and weak n–π* (~430 nm) absorbance in the ultraviolet (UV) and visible (vis) regions, respectively. The photoswitching (*E*→*Z*) of **1** and **2** was performed under 365 nm UV and 405 nm vis light irradiation, respectively. The π–π* transition band of *Z* isomers shifts toward a shorter wavelength, accompanied by a considerable decrease in intensity, and the intensity of the n–π* band increases. In acetonitrile at 360 nm photostationary state (PSS), *E*→*Z* conversion was 95% and 89% for **1** and **2**, respectively (Figures S3 and S4). The reverse photoisomerization was achieved under 525 nm light irradiation (*Z*→~75% of *E*-**1** or *E*-**2**). **1** and **2** show slow thermal reverse isomerization in acetonitrile (Figure 1f) but a relatively fast thermal reverse isomerization in water. The *Z*→*E* thermal back half-life ($t_{1/2}$) of **1** and **2** are 9.6 min and 14.7 s at 37 °C in an aqueous medium, respectively (Figures S5 and S6). **1** and **2** are highly robust, which exhibit several photoisomerization cycles without fatigue (Figures 1e and S1). Theoretical calculation predicted a straight *E* isomer and bent *Z* isomer with two aromatic rings partly facing each other in the ground state (Figure 1d; Tables S5 and S6). *E* and *Z* isomers of **1** and **2** are

stable in aqueous media containing 1 mM glutathione, an intracellular reductant. (Figure S7).

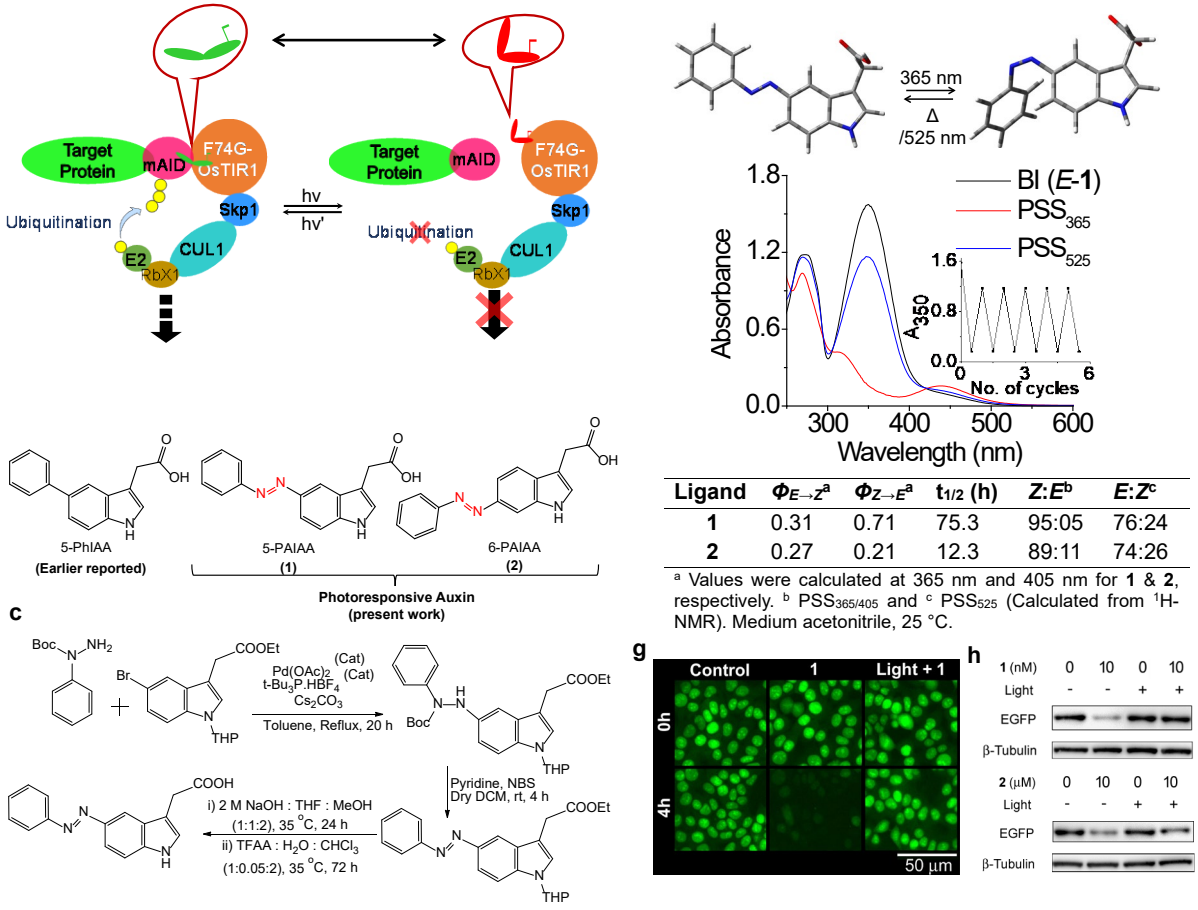

Ligand	$\Phi_{E\rightarrow Z}$[a]	$\Phi_{Z\rightarrow E}$[a]	$t_{1/2}$ (h)	Z:E[b]	E:Z[c]
1	0.31	0.71	75.3	95:05	76:24
2	0.27	0.21	12.3	89:11	74:26

[a] Values were calculated at 365 nm and 405 nm for **1** & **2**, respectively. [b] $PSS_{365/405}$ and [c] PSS_{525} (Calculated from ^{1}H-NMR). Medium acetonitrile, 25 °C.

Figure 1. Photoswitchable auxin for conditional protein degradation. a) On–off conditional protein degradation with photoswitchable molecular glue. b) Design and c) synthesis of photoresponsive auxin. d) Isomerization condition and structural dissimilarity (ground state optimized geometry) of *E* and *Z* photoisomers of **1**. e) Absorption spectra of **1** in acetonitrile at 25 °C before light irradiation at different PSSs. The photostability of photoisomerized ligands (inset). f) Photoisomerization quantum yield (Φ), $Z\rightarrow E$ $t_{1/2}$, and the ratio of *E* and *Z* isomers in the PSS of **1** and **2** in acetonitrile at 25 °C. g) Fluorescence microscopy of HAP1 cells expressing $OsTIR1^{F74G}$ and mAID–EGFP–NLS before and after 4 h treatment with DMSO (control) and 10 nM **1** in dark and illuminated conditions. h) Western blot of mAID–EGFP–NLS (detected using anti-EGFP antibody) with **1** and **2** in dark and light conditions. β-tubulin was used as a loading control.

We treated HAP1 cell stably expressing $OsTIR1^{F74G}$ and a mAID-fused enhanced green-fluorescent protein with a nuclear-localization signal (mAID–EGFP–NLS) reporter[6,17,19,20] with dimethyl sulfoxide (DMSO; control), **1**, or **2** for 4 h at 37 °C in dark and light to test the gluing ability of the ligands. A 365 nm light with 0.2-mW cm^{-2} intensity and a 405-nm light with 0.8 mW cm^{-2} intensity were used to irradiate **1** and **2**, respectively, to maintain the *Z*-rich PSS without affecting cell viability. GFP signal intensity decreases in the dark in the presence of 10 nM **1** or 10 µM **2** (Figures 1g and S8). Western blot analysis confirms the degradation of mAID–EGFP–NLS by **1** and **2** (Figure 1h). By contrast, the *Z*-rich PSS is remarkably less efficient to diminish the GFP signal intensity with the same ligand concentrations in light. We measured the GFP intensity using a flow cytometer to quantify the molecular glue effect of ligands in dark and light. GFP intensity decreases in a dose-dependent manner (Figures 2a and 2b). In the dark, 1.26 nM of **1** accomplished 50% of the maximum GFP degradation (EC_{50}). By contrast, the EC_{50} for the *Z*-rich PSS of **1** was 410 nM. We hypothesized that only *E*-**1** with 5% concentration would degrade the protein in the *Z*-rich PSS, while *Z*-**1** with 95% concentration had no effect. Thus, we used the experimental data from 100% *E*-**1** (represented by the black line) to derive the theoretical curve of 5% *E*-**1**, resulting in the blue line with an EC_{50} of 24.90 nM. However, this deviates from the results obtained in the *Z*-rich PSS experiment (represented by the red line). We were compelled to consider the possibility that *Z*-**1** is recognized in the auxin binding pocket and acts as a competitive inhibitor of *E*-**1** in protein degradation to explain this discrepancy. We verified the antagonist nature of the *Z*-**1** with two additional activity curves in the presence of 2 nM or 12 nM of *Z*-**1** derived by generating various *E*/*Z* isomer ratios at PSS_{365}, PSS_{405}, PSS_{430}, PSS_{470} and PSS_{525} (Figure S9, Tables S2 and S3). The activity curve was shifted towards higher agonist (*E*-**1**) concentrations as the *Z*-**1** concentration increased from 0 nM to 2 nM and then to 12 nM (Figure S10). Utilizing the Schild method, we approximated the K_d value of *Z*-**1** as an antagonist to be around 1-2 nM (Table S4). The *E*-agonist/*Z*-antagonist nature results in an exceptional ~325-fold switching of the corresponding EC_{50} values.[21] The de novo PAID system achieved ~84% difference in protein degradation using 10-nM

1 (Figure S11). The EC_{50} of **2** is 6.42 and 18.46 µM in dark and light, respectively.

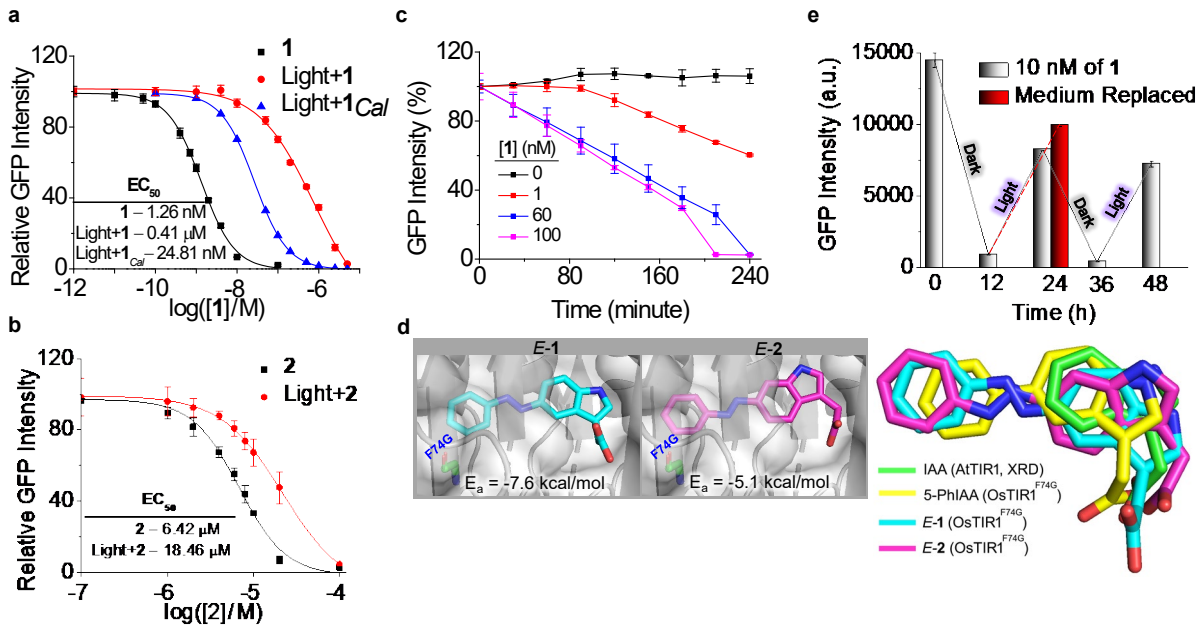

Figure 2. Properties and functionality of PAID technology. Depletion of mAID–EGFP–NLS in HAP-1 cell with a) **1** and b) **2** in the absence (black) and presence (red) of light. Calculated degradation of mAID–EGFP–NLS with 5% of *E*-**1** in PSS_{365} is shown as a blue line (assuming *Z*-**1** isomer is completely inefficient to form the $OsTIR1^{F74G}$-*Z*1–POI ternary composite). Mean ± S.D., n = 3. The EC_{50} values are shown in the inset. c) Effectiveness of PAID technology for conditional protein degradation in different conditions. Mean ± S.D., n = 3. d) Molecular docking of *E* isomer of **1** and **2** with $OsTIR1^{F74G}$. E_a represents binding affinity. Docked poses of 5-PhIAA (yellow), *E*-**1** (cyan), and *E*-**2** (magenta) inside $OsTIR^{F74G}$ superimposed with IAA (green) in IAA–AtTIR1. X-ray crystal structure (PDB–2PIQ) are displayed on the left. e) Temporal resolution: the GFP re-expression/degradation controlled with on–off light irradiation. The red bar shows the GFP re-expression after removing **1** (medium replacement). Mean ± S.D., n = 3.

The protein degradation with photoswitchable auxins is entirely blocked in the presence of a proteasome inhibitor MG-132 (Figure S12), indicating that the protein depletion follows a proteasomal pathway. The molecular glue was not toxic to the cells within the specific working concentrations (Figure S13). The effectiveness of the PAID system at various concentrations of **1** was estimated by monitoring the GFP expression level at different reaction times. Figure 2c shows a linear decay of the GFP intensity with time. The slope becomes steeper at higher ligand concentrations. This pseudo-zeroth-order kinetics appear owing to the high substrate concentration than that of the $OsTIR1^{F74G}$-molecular glue composite concentration.[22] 50% POI was degraded in 129 ± 2 min (reaction $T_{1/2}$) with 100 nM *E*-1.

Molecular docking was performed to elucidate the binding nature of different isomers within $OsTIR1^{F74G}$ (Figures 2d and S14). The 3D structures of OsTIR1 (GeneID-4335696) and $OsTIR1^{F74G}$ (the phenylalanine at the 74th position was replaced with glycine in the GeneID-4335696) proteins were developed with homology model using SWISS-MODEL from AtTIR1 (PDB-2P1M) as a template (61% identities) with good QMEAN score (Figures S15 and S16). The phenyl moiety (bump) of *E* isomers entered the F74G pocket (hole). *E* isomers were docked inside the auxin binding pocket. The binding of the IAA moiety of *E*-**1** and *E*-**2** were similar to the IAA ligand binding observed in the IAA–AtTIR1 crystal (Figures 2d and S17).[23] The predicted binding affinities of *E*-**1** and *E*-**2** from docking simulation are −7.6 and −5.1 kcal mol^{-1}, respectively. The difference in the binding energy correlates well with experimental results. *Z* isomers showed a different orientation inside the binding pocket (Figure S14). The bent structure of the *Z* isomers prevented the phenyl ring to dock inside the F74G pocket. The binding affinities of *Z*-**1** and *Z*-**2** are −8.0 and −7.4 kcal mol^{-1}, respectively. It should be noted that the stability of the ternary composite (OsTIR1-molecular glue–target protein) ultimately regulates the catalytic protein degradation. Our theoretical findings corroborate the *E*-agonist/*Z*-antagonist nature of the photoswitch.

We selected **1** to study the spatiotemporal resolution of the PAID system because of higher photoswitchable gluing efficiency. The PAID system can be reversibly switched on–off by maintaining a dark or illuminated condition for multiple times without affecting the glue efficiency. The POI is re-expressed by replacing the medium with a molecular glue-free medium after protein degradation.[3,4,7,17] We tested the GFP degradation/re-expression of **1** in 12 h dark/light conditions (Figure 2e). ~95% proteins were degraded in 4 h in dark, after which the state was maintained. The protein degradation ceased in light, and the natural protein re-expression predominated. The protein re-expression in the presence of light shows similar result to that of solvent replacement (Figure 2e).

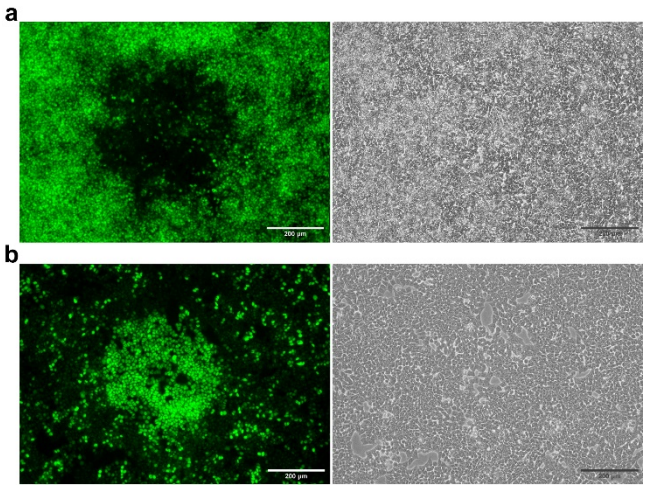

Figure 3. Spatial resolution of the PAID system obtained with a) 150 nM **1** with a 525 nm focal irradiation at the bottom and 365 nm global irradiation at the top, b) 60 nM **1** and only 365 nm focal irradiation at the bottom. Left panels show fluorescence microscopy of mAID-EGFP-NLS. The bright field images on the right display the cell distribution. Scale bar 200 µm.

We illuminated 525 nm light for 4 h on a tiny focal area (diameter/length ~350 µm) and 365 nm light on the whole area (Figure S21a) of the sample containing 150 nM **1** to demonstrate spatial resolution. A GFP signal is conspicuously absent in the central circular region, while a robust GFP signal is present in the surrounding background. (Figure 3a, S18b). **1** diffuses in the sample but the circular region illuminated by 525 nm light is photoisomerized from *Z*-**1** to *E*-**1** maintaining an *E*-rich PSS. Alternately, the background light at 365 nm induces the photoisomerization from *E*-**1** to *Z*-**1**, maintaining a *Z*-rich PSS in other regions. Thus, the GFP of cells is decomposed in a limited area of ~350 µm without affecting the other areas. Figure 3b shows the undecomposed GFP signal of the cell obtained by continuously irradiating ~350 µm area using 365 nm light (Figure S21b). This high contrast is obtained without irradiating the background under 525 nm light (Compare Figure 3b with Figure S19). **1** photoisomerized from *E*-**1** to *Z*-**1** in the 365 nm light-irradiated area, maintaining the *Z*-rich PSS without the decomposition of the GFP signal. *Z*-**1** generated in this area diffuses into the background, but the lifetime of *Z*-**1** in the buffer medium is shorter than that of the protein degradation rate, and *Z*-**1** thermally returns to *E*-**1**. As a result, the *E*-rich state is maintained in the background. Thus, a high contrast of the GFP signal is obtained even under a single wavelength. Our control experiments have demonstrated that the degradation of the target protein at specific sites is not simply a photobleaching process, which is facilitated by direct absorption by GFP or assisted by azobenzene (Figure S20).

In conclusion, we developed a PAID system for rapid and conditional protein degradation with spatiotemporal resolution. The binding of the bump inside the OsTIR1^{F74G} hole strictly controlled the gluing efficiency, depending on ligand's isomer structures. Different gluing abilities of *E* and *Z* isomers enabled the photoswitch to work reversibly in an agonist/antagonist manner in dark/light conditions with a 325-fold difference in EC_{50} values. We believe that adding spatiotemporal resolution and an on–off switch will improve the present AID system in studying protein functionalities and highly dynamic biological processes such as cell cycles, neuronal signaling, or immune response in multicellular systems.

ASSOCIATED CONTENT

Supporting Information. Experimental methods, synthesis protocols, NMR spectra, photoisomerization behavior, ground state optimized geometry, effect of reduced glutathione, protein ligand interaction from molecular modeling, cell culture, cytotoxicity assay are provided in the supporting information.

AUTHOR INFORMATION

Corresponding Author

*Nobuyuki Tamaoki - Research Institute for Electronic Science, Hokkaido University, Kita20, Nishi 10, Kita-ku, Sapporo, Hokkaido 001-0020, Japan; Graduate School of Life Science, Hokkaido University, Kita 10, Nishi 8, Kita-ku, Sapporo, Hokkaido 060-0810, Japan; ORCID https://orcid.org/0000-0003-1079-7087; Email: tamaoki@es.hokudai.ac.jp

Funding Sources

This work was financially supported by KAKENHI Grants-in-Aid for Scientific Research B (no. 22H02153 to N.T and no. 24K02017 to R.U.).

Notes

The authors declare no competing financial interest.

ACKNOWLEDGMENT

We thank the Open Facility, Global Facility Center, Creative Research Institution, Hokkaido University for use of the FACSCanto flow cytometer.

REFERENCES

(1) Natsume, T.; Kanemaki, M. T. Conditional Degrons for Controlling Protein Expression at the Protein Level. *Annu. Rev. Genet.* **2017**, *51*, 83-102. DOI: 10.1146/annurev-genet-120116-024656.

(2) Kanemaki, M. T. Ligand-Induced Degrons for Studying Nuclear Functions. *Curr. Opin. Cell Biol.* **2022**, *74*, 29-36. DOI: 10.1016/j.ceb.2021.12.006.

(3) Nishimura, K.; Fukagawa, T.; Takisawa, H.; Kakimoto, T.; Kanemaki, M. An Auxin-Based Degron System for the Rapid Depletion of Proteins in Nonplant Cells. *Nat. Methods* **2009**, *6*, 917-922. DOI: org/10.1038/nmeth.1401.

(4) Holland, A. J.; Fachinetti, D.; Han, J. S.; Cleveland, D. W. Inducible, Reversible System for the Rapid and Complete Degradation of Proteins in Mammalian Cells. *Proc. Natl. Acad. Sci. U.S.A.* **2012**, *109* (49), E3350-E3357. DOI: 10.1073/pnas.1216880109/suppl_file/sm08.avi.

(5) Zhang, L.; Ward, J. D.; Cheng, Z.; Dernburg, A. F. The Auxin-Inducible Degradation (AID) System Enables Versatile Conditional Protein Depletion in C. Elegans. *Dev.* **2015**, *142* (24), 4374-4384. DOI: 10.1242/dev.129635/256908/am/the-auxin-inducible-degradation-aid-system-enables.

(6) Natsume, T.; Kiyomitsu, T.; Saga, Y.; Kanemaki, M. T. Rapid Protein Depletion in Human Cells by Auxin-Inducible Degron Tagging with Short Homology Donors. *Cell Rep.* **2016**, *15* (1), 210-218. DOI:

10.1016/j.celrep.2016.03.001.

(7) Hoffmann, S.; Dumont, M.; Barra, V.; Ly, P.; Nechemia-Arbely, Y.; McMahon, M. A.; Hervé, S.; Cleveland, D. W.; Fachinetti, D. CENP-A Is Dispensable for Mitotic Centromere Function after Initial Centromere/Kinetochore Assembly. *Cell Rep.* **2016**, *17* (9), 2394-2404. DOI: 10.1016/j.celrep.2016.10.084.

(8) Nora, E. P.; Goloborodko, A.; Valton, A. L.; Gibcus, J. H.; Uebersohn, A.; Abdennur, N.; Dekker, J.; Mirny, L. A.; Bruneau, B. G. Targeted Degradation of CTCF Decouples Local Insulation of Chromosome Domains from Genomic Compartmentalization. *Cell* **2017**, *169* (5), 930-944.e22. DOI: 10.1016/j.cell.2017.05.004.

(9) Lu, Z.; Peng, B.; Ebert, B. E.; Dumsday, G.; Vickers, C. E. Auxin-Mediated Protein Depletion for Metabolic Engineering in Terpene-Producing Yeast. *Nat. Commun.* **2021**, *12* (1051), 1-13. DOI: 10.1038/s41467-021-21313-1.

(10) Capece, M.; Tessari, A.; Mills, J.; Vinciguerra, G. L. R.; Louke, D.; Lin, C.; McElwain, B. K.; Miles, W. O.; Coppola, V.; Davies, A. E.; Palmieri, D.; Croce, C. M. A Novel Auxin-Inducible Degron System for Rapid, Cell Cycle-Specific Targeted Proteolysis. *Cell Death Differ.* **2023**, *30* (9), 2078-2091. DOI: 10.1038/s41418-023-01191-4.

(11) Mafy, N. N.; Matsuo, K.; Hiruma, S.; Uehara, R.; Tamaoki, N. Photoswitchable CENP-E Inhibitor Enabling the Dynamic Control of Chromosome Movement and Mitotic Progression. *J. Am. Chem. Soc.* **2020**, *142* (4), 1763-1767. DOI: 10.1021/jacs.9b12782/asset/images/large/ja9b12782_0004.jpeg.

(12) Amrutha, A. S.; Kumar, K. R. S.; Kikukawa, T.; Tamaoki, N. Targeted Activation of Molecular Transportation by Visible Light. *ACS Nano* **2017**, *11* (12), 12292-12301. DOI: 10.1021/acsnano.7b06059/asset/images/large/nn-2017-060599_0006.jpeg.

(13) Kobauri, P.; Dekker, F. J.; Szymanski, W., Feringa, B. L. Rational Designin Photopharmacology with Molecular Photoswitches *Angew. Chem. Int. Ed.* **2023**, *62*, e202300681. DOI:10.1002/anie.202300681.

(14) Pfaff, P.; Samarasinghe, K. T. G.; Crews, C. M.; Carreira, E. M. Reversible Spatiotemporal Control of Induced Protein Degradation by Bistable PhotoPROTACs. *ACS Cent. Sci.* **2019**, *5* (10), 1682-1690. DOI: 10.1021/acscentsci.9b00713/asset/images/large/oc9b00713_0005.jpeg.

(15) Reynders, M.; Matsuura, B. S.; Bérouti, M.; Simoneschi, D.; Marzio, A.; Pagano, M.; Trauner, D. PHOTACs Enable Optical Control of Protein Degradation. *Sci. Adv.* **2020**, *6* (8). DOI: 10.1126/sciadv.aay5064/suppl_file/aay5064_sm.pdf.

(16) Zhang, Q.; Kounde, C. S.; Mondal, M.; Greenfield, J. L.; Baker, J. R.; Kotelnikov, S; Ignatov, M.; Tinworth, C. P.; Zhang, L.; Conole, D.; De Vita, E.; Kozakov, D.; McCluskey, A.; Harling, J. D.; Fuchter, M. J.; Tate, E. W. Light-mediated multi-target protein degradation using arylazopyrazole photoswitchable PROTACs (AP-PROTACs) *Chem. Commun.* **2022**, *58* (24), 10933-10936. DOI: 10.1039/d2cc03092f.

(17) Arp, C. J.; Reynders, M.; Sreekanth, V.; Kokkonda, P.; Pagano, M.; Choudhary, A.; Trauner, D. Photoswitchable Molecular Glues Enable Optical Control of Transcription Factor Degradation. *bioRxiv* **2023**, 2023.04.09.536172. DOI:10.1101/2023.04.09.536172.

(18) Yesbolatova, A.; Saito, Y.; Kitamoto, N.; Makino-Itou, H.; Ajima, R.; Nakano, R.; Nakaoka, H.; Fukui, K.; Gamo, K.; Tominari, Y.; Takeuchi, H.; Saga, Y.; Hayashi, K. ichiro; Kanemaki, M. T. The Auxin-Inducible Degron 2 Technology Provides Sharp Degradation Control in Yeast, Mammalian Cells, and Mice. *Nat. Commun.* **2020**, *11* (5701), 1-13. DOI: 10.1038/s41467-020-19532-z.

(19) Uchida, N.; Takahashi, K.; Iwasaki, R.; Yamada, R.; Yoshimura, M.; Endo, T. A.; Kimura, S.; Zhang, H.; Nomoto, M.; Tada, Y.; Kinoshita, T.; Itami, K.; Hagihara, S.; Torii, K. U. Chemical Hijacking of Auxin Signaling with an Engineered Auxin–TIR1 Pair. *Nat. Chem. Biol.* **2017**, *14* (3), 299-305. DOI: 10.1038/nchembio.2555.

(20) Yunusova, A.; Smirnov, A; Shnaider, T; Lukyanchikova, V; Afonnikova, S; Battulin, N. Evaluation of the OsTIR1 and AtAFB2 AID Systems for Genome Architectural Protein Degradation in Mammalian Cells. *Front. Mol. Biosci.* **2021**, 8, 757394. DOI: 10.3389/fmolb.2021.757394.

(21) Hansen, M. J.; Hille, J. I. C.; Szymanski, W.; Driessen, A. J. M.; Feringa, B. L. Easily Accessible, Highly Potent, Photocontrolled Modulators of Bacterial Communication. *Chem* **2019**, 5 (5), 1293–1301. DOI: 10.1016/j.chempr.2019.03.005.

(22) Atkins, P. W., de Paula J., K. J. *Physical Chemistry*, 11th ed. Oxford University Press, 2017; pp 944.

(23) Tan, X.; Calderon-Villalobos, L. I. A.; Sharon, M.; Zheng, C.; Robinson, C. V.; Estelle, M.; Zheng, N. Mechanism of Auxin Perception by the TIR1 Ubiquitin Ligase. *Nat.* **2007**, *446* (7136), 640–645. DOI: 10.1038/nature05731.

TOC graphic

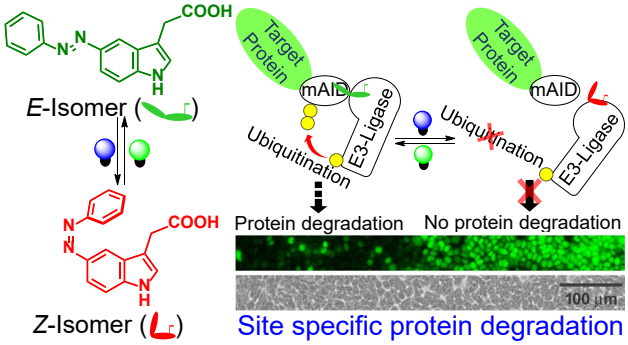
COOH
E-Isomer
Z-Isomer
COOH
Target Protein
mAID
E3-Ligase
Ubiquitination
Protein degradation
Target Protein
mAID
E3-Ligase
Ubiquitination
No protein degradation
100 μm
Site specific protein degradation